(Received 21 June 2025, Accepted 18 July 2025, Scheduled 2 August 2025)

Compact Self-Decoupled MIMO Antenna Based on Current Cancellation for UAVs

Yang-Yang Guan[1], Peng Zhang[1], Xu-Long Wang[2,*], and Jie Bai[2]

[1] *National Key Laboratory of Electromagnetic Information Control and Effects Shenyang Aircraft Design and Research Institute, Shenyang, China*
[2] *School of Electronic Engineering, Xidian University, Xi'an, China*

ABSTRACT: In this paper, a compact multiple-input multiple-output (MIMO) antenna is proposed for unmanned aerial vehicles (UAVs). By simultaneously exciting common mode (CM) and differential mode (DM) from a T-shaped slot, wideband coverage is achieved. Four such slot antennas are used to form a four-antenna module operating in the N79 band (4.4–5.0 GHz). The size of the four-antenna module is merely 43×8 mm^2, demonstrating excellent miniaturization and integration. The dominant coupling between adjacent elements occurs through currents of the same mode. When CM and DM currents coexist, partial cancellation of coupled currents at the feed point enables high isolation without external decoupling structures. Two modules are symmetrically positioned along the longer edges of the frame, forming an 8-element MIMO antenna. The antenna achieves isolation greater than 11 dB and envelope correlation coefficient (ECC) below 0.04. The measured total efficiency is better than 52%, with an average of 56%. Featuring compact footprint, zero-clearance constraint and high isolation, the proposed antenna is a promising candidate for 5G UAVs.

1. INTRODUCTION

The transmission rate and communication quality of 5G wireless communication systems have been steadily improving. As one of the key technologies of 5G, multiple-input multiple-output (MIMO) technology [1] significantly enhances communication quality and reliability through the multipath propagation advantages of diversity techniques [2], while also improving spectral efficiency and expanding channel capacity through multiplexing methods [3]. Due to its outstanding performance, MIMO technology is increasingly deployed in various 5G terminals, among which unmanned aerial vehicles (UAVs) stand out as a prominent application. UAVs are characterized by stringent size, weight, and power constraints, yet they require high-capacity and reliable wireless links, making the design of efficient and compact MIMO antenna particularly critical. As the number of antenna elements increases, the channel capacity of the MIMO antenna is significantly enhanced. However, the limited installation space on such platforms leads to strong electromagnetic coupling among antenna elements, which degrades radiation performance and reduces the MIMO antenna channel capacity [4]. Therefore, designing multi-element, low-coupling MIMO antenna has become a key development trend for future 5G terminal antennas.

Increasing the distance between antenna elements or strategically placing antennas to achieve spatial diversity and high isolation is the most straightforward design approach [5]. However, due to the compact nature of terminal devices, the effectiveness of this method is limited. A commonly adopted solution is to add decoupling structures between elements. Isolation performance can be further improved by incorporating neutralization lines [6–8], parasitic structures [9–11], decoupling networks [12–14], and defected ground structures (DGSs) [15, 16]. With the ongoing trend toward miniaturization and lightweight design of UAVs, the available space for antenna integration is increasingly constrained, and the additional footprint introduced by decoupling structures poses challenges to compact antenna design.

To address this, a self-decoupling design approach for tightly spaced, high-isolation antenna pairs is proposed. In antenna pair design, traditional methods such as mode orthogonality [17–22] and polarization orthogonality [23, 24] require modal analysis of specific structures to identify decoupling mechanisms, making the design process relatively complex. For example, in [18], a feeding network is designed to excite two sets of orthogonal characteristic modes in a dual-antenna pair, achieving isolation greater than 20 dB in the 3.3-3.8 GHz band. In [23], a polarization-orthogonal dual antenna pair is presented in which both antennas share a common radiating structure. Ant 1 excites an in-phase current mode that generates Y-polarized radiation, while Ant 2 excites a slot mode that generates X-polarized radiation. The antenna elements thus exhibit polarization orthogonality, with isolation greater than 24.1 dB between the dual antenna pair.

Subsequent research has proposed and validated the orthogonality between common mode (CM) and differential mode (DM) current distributions [25], and employed their cancellation to achieve high isolation in antenna pairs [26]. However, adequate spacing between antenna pairs is still required to meet the isolation requirements of MIMO arrays. To fulfill the demands for high channel capacity and compact antenna design in

* Corresponding author: Xu-Long Wang (24021211421@stu.xidian.edu.cn).

5G terminal applications, the development of self-decoupling multi-element antenna module is of significant importance.

In this paper, a compact self-decoupled MIMO antenna based on CM and DM current partial cancellation is proposed for UAVs. By using characteristic mode analysis to excite CM and DM currents from the antenna elements, a four-antenna module measuring $43 \times 8\,\text{mm}^3$ is designed to cover the N79 band (4.4–5.0 GHz). At the low-frequency resonance, the elements operate in DM, while at the high-frequency resonance, they operate in CM. The electromagnetic coupling between adjacent antenna elements generates coupled currents of the same mode. Within the operating frequency band, both modes coexist, and the partially out-of-phase coupled currents effectively cancel each other at the feed point, thereby achieving high isolation. Two sets of four-antenna modules are distributed on two side frames to form an eight-element MIMO antenna system. The proposed design achieves isolation better than 11 dB and envelope correlation coefficient (ECC) below 0.04. The total efficiency exceeds 52%, with an average efficiency of 56%.

2. ANTENNA ELEMENT DESIGN

The detailed structure of the proposed antenna element is illustrated in Figure 1. A $150 \times 75 \times 0.8\,\text{mm}^3$ FR-4 substrate ($\varepsilon_r = 4.4$, $\tan\delta = 0.02$) is used, with its bottom side fully metallized to serve as the ground plane. An FR-4 frame with dimensions of $150 \times 8 \times 0.8\,\text{mm}^3$ is vertically mounted along one longer edge of the ground plane. The substrate is positioned centrally within the frame, and a metallic layer is printed on the upper section of the inner surface. The antenna element consists of a T-shaped slot etched on the inner surface of the frame, along with a metallic boundary that forms part of the radiating structure.

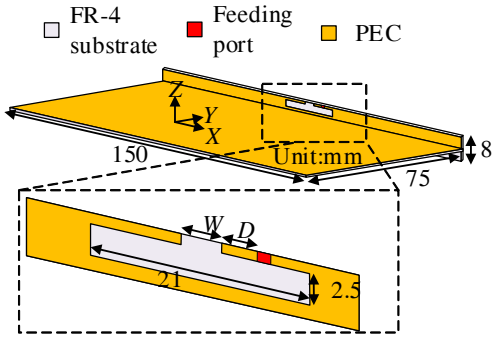

FIGURE 1. The proposed geometry of the antenna element.

To illustrate the design concept of the T-shaped slot antenna, its reference structure is shown in Figure 2. Based on characteristic mode theory, the antenna supports a set of orthogonal modal currents, and CM and DM can be effectively excited through appropriately designed feeding structures, enabling the realization of a dual-resonant antenna with both CM and DM resonances.

Characteristic mode analysis is performed on the reference antenna, and the modal significances of the five dominant modes are shown in Figure 2. At frequencies above 3.0 GHz, the modal significances of all five modes are greater than $1/\sqrt{2}$,

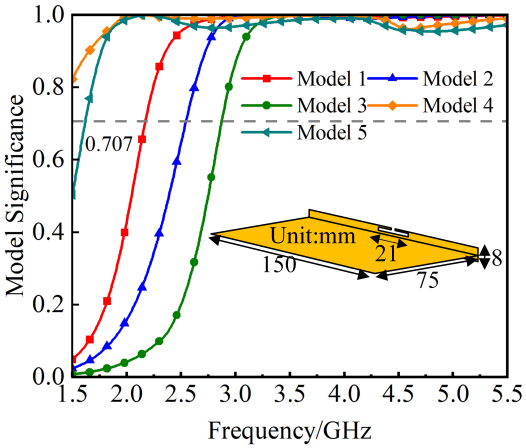

FIGURE 2. The mode significance of the dominant 5 modes for the reference antenna.

indicating that they can be efficiently excited. At 3.5 GHz, the current distributions of the five dominant modes are illustrated in Figure 3, where red dots indicate regions with the strongest current density. It is observed that modes 2, 4, and 5 have currents distributed along the entire vertical metallic frame, whereas modes 1 and 3 have currents primarily concentrated around the T-shaped slot. Since extensive radiation from the metallic frame negatively impacts the isolation between antenna elements, modes 1 and 3 are selected as the desired modes. The current distribution of mode 1 corresponds to CM, characterized by in-phase currents with similar amplitudes on both sides of the slot. In contrast, the reference antenna exhibits DM current distribution at mode 3, in which the current directions on two sides of the T-shaped slot are opposite, and the current amplitudes are approximately equal. By placing voltage sources at the locations with maximum modal current, mode 1 and mode 3 are effectively excited.

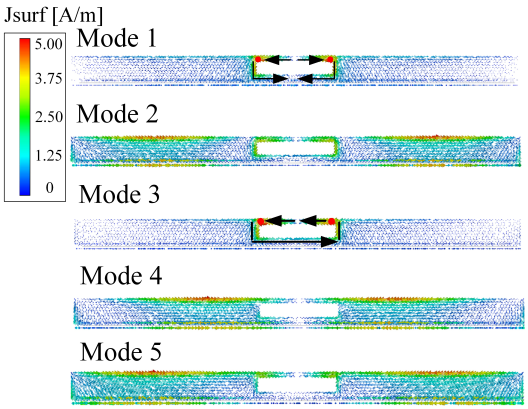

FIGURE 3. Mode current distribution of the dominant 5 modes at 3.5 GHz.

In Figure 4, the proposed antenna exhibits a −6 dB impedance bandwidth of 660 MHz (4.08–4.74 GHz), demonstrating dual resonant characteristics at 4.3 GHz (DM) and 4.6 GHz (CM). The antenna currents are well confined around the T-shaped slot, while the current on the overall metal frame remains weak. Notably, the strong current is primarily concen-

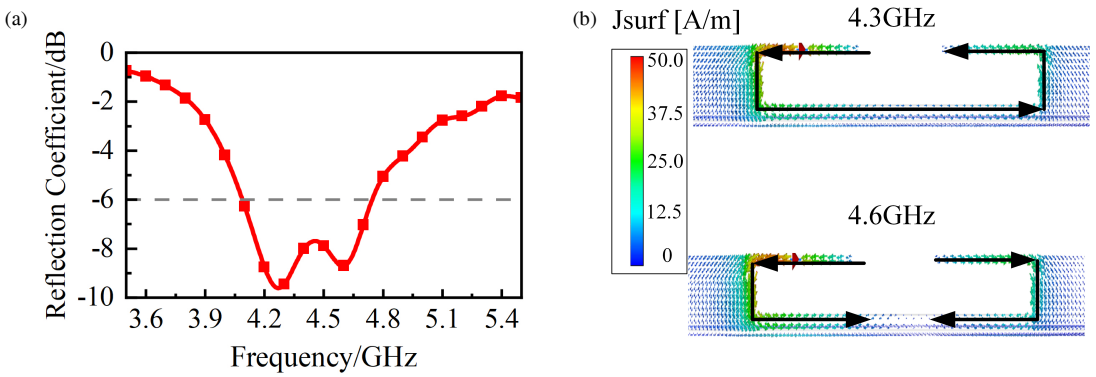

FIGURE 4. (a) Reflection coefficient of the antenna; (b) Current distribution at 4.3 GHz and 4.6 GHz.

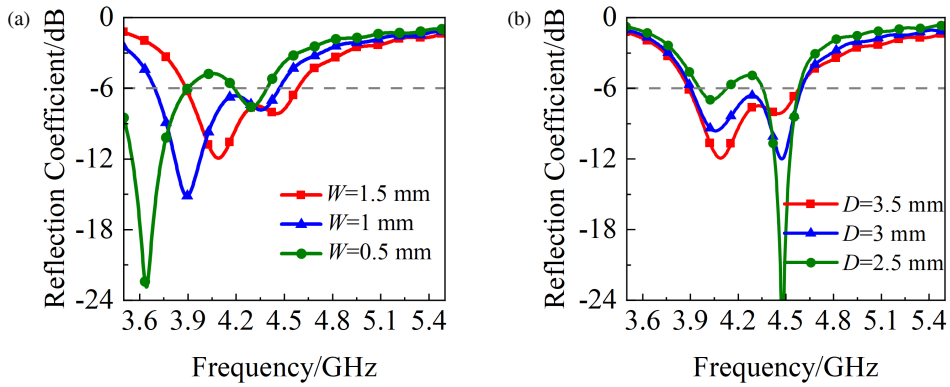

FIGURE 5. Reflection coefficient as a function of (a) W and (b) D.

trated at the feed position. Furthermore, to effectively control the impedance bandwidth and mode resonance excitations of the antenna, a comprehensive analysis of the key design parameters was conducted.

The effects of the slot width W and the distance D between the feed point and slot aperture on the antenna performance are investigated in the following analysis. Keeping other parameters constant, Figure 5 presents the variation of the reflection coefficient with respect to W and D. As W decreases, both resonance frequencies shift to lower values, and the impedance matching at the low-frequency resonance improves. In contrast, decreasing D improves the impedance matching at the high-frequency resonance but deteriorates it at the low-frequency resonance. By adjusting W, the frequency spacing between the two resonances can be effectively controlled. Meanwhile, selecting an appropriate value for D allows for the optimization of impedance matching at both resonances. When W is set to 1.5 mm and D set to 3.5 mm, the antenna achieves good impedance matching over a wide bandwidth.

3. FOUR-ANTENNA MODULE

3.1. Antenna Configuration

The aforementioned antenna elements are arranged in a compact configuration to form a four-antenna module, as illustrated in Figure 6. All four elements share the same structural design. Ant 1 and Ant 2, together with Ant 3 and Ant 4, are vertically

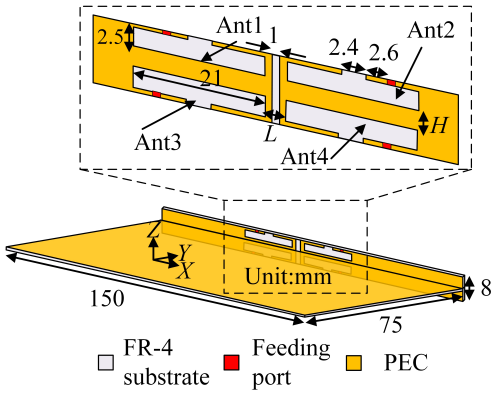

FIGURE 6. Structure of the proposed four-antenna module, where $L = 5$ mm and $H = 2$ mm.

symmetric with respect to the center of the frame, while Ant 1 and Ant 3, as well as Ant 2 and Ant 4, are horizontally symmetric. Slight adjustments were made to the slot width and the distance between the feed point and slot aperture. A vertical slot etched at the center of the module was introduced to enhance isolation, resulting in a more compact overall footprint.

3.2. Decoupling Mechanism

The key decoupling mechanism is explained through the analysis of surface current distributions. Due to the symmetry in the antenna layout, only the decoupling mechanisms between

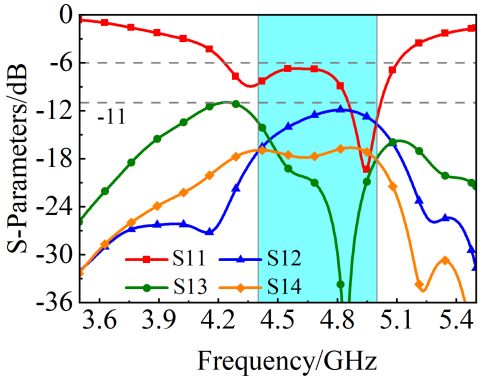

FIGURE 7. S-parameters of the proposed four-antenna module.

selected antenna elements are described. Figure 7 presents the S-parameters of the proposed four-antenna module. Due to the structural symmetry, only a subset of S-parameters is shown. It can be observed that Ant 1 exhibits two resonant frequencies at 4.3 GHz and 4.9 GHz, with a -6 dB impedance bandwidth ranging from 4.4 GHz to 5.0 GHz. The isolation between antenna elements exceeds 11 dB across the entire operating band. Certainly, when the platform design affords greater spatial flexibility, a trade-off can be achieved between port isolation and antenna dimensions. By increasing both the transverse spacing (L) and longitudinal spacing (H) between antenna elements, the near-field coupling effects can be further attenuated, thereby reducing mutual interference and enhancing isolation performance to meet practical application requirements.

Figure 8 shows the surface current distributions when Ant 1 is excited and Ant 2 terminated, at 4.3, 4.6, and 4.9 GHz. At 4.3 GHz, the surface currents on both sides of the slot on Ant 1 are out-of-phase with similar amplitudes, indicating DM. The coupled current on Ant 2 also exhibits DM distribution. At 4.9 GHz, the surface currents are in-phase with similar amplitudes, indicating CM, and the coupled current on Ant 2 also exhibits CM. At 4.6 GHz, where the working frequencies of CM and DM modes overlap, both modes coexist. The surface current on Ant 1 and the coupled current on Ant 2 are superpositions of CM and DM. Due to partial cancellation between the two modes, the net coupled current at the feed point of Ant 2 is reduced. This leads to a high isolation between closely spaced Ant 1 and Ant 2 without introducing any additional decoupling structure.

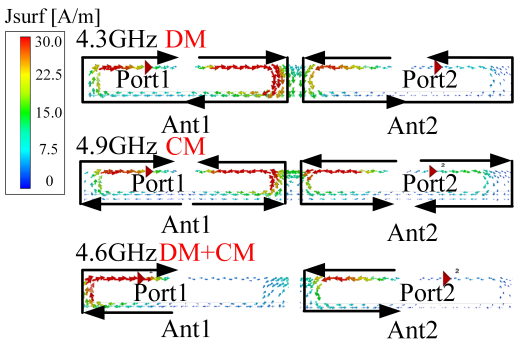

FIGURE 8. Surface current distributions at 4.3, 4.6, and 4.9 GHz when Ant 1 is excited and Ant 2 is terminated.

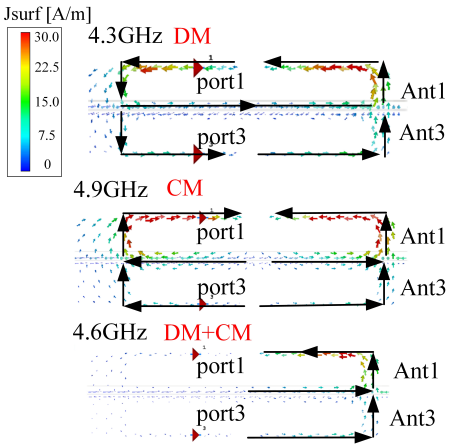

FIGURE 9. Surface current distributions at 4.3, 4.6, and 4.9 GHz when Ant 1 is excited and Ant 3 is terminated.

Similarly, in Figure 9, Ant 1 operates in DM, and the coupled current on Ant 3 also exhibits DM at 4.3 GHz. At 4.9 GHz, both operate in CM with similar characteristics. At 4.6 GHz, a superposition of CM and DM causes partial cancellation, reducing the coupled current at the feed point of Ant 3 and improving isolation despite the compact layout. Overall, this decoupling method improves the utilization of the limited design space, making it suitable for compact 5G terminal applications.

4. SIMULATED AND MEASURED RESULTS

To verify the performance of the proposed antenna module, two modules are symmetrically arranged along the longer edges of the supporting frame, resulting in an 8-element MIMO antenna. As illustrated in Figure 10, the antenna is implemented on a $150 \times 75 \times 0.8\,\text{mm}^3$ FR-4 substrate with a fully printed metallic ground plane on its bottom side. To validate the feasibility of the proposed design, a prototype was fabricated and measured. The MIMO antenna is fed using 50-ohm SMA coaxial connectors, as shown in Figure 11. The antenna was fully simulated

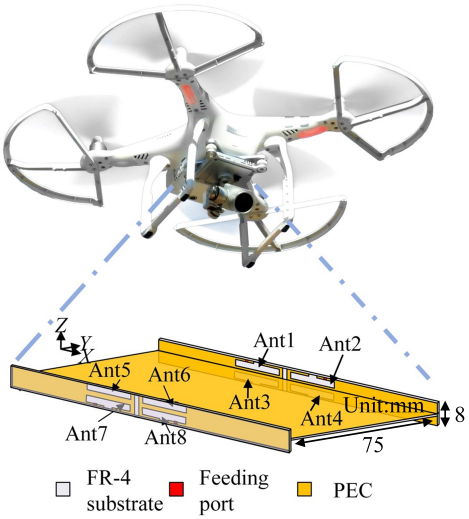

FIGURE 10. Geometry of the proposed eight-element MIMO antenna.

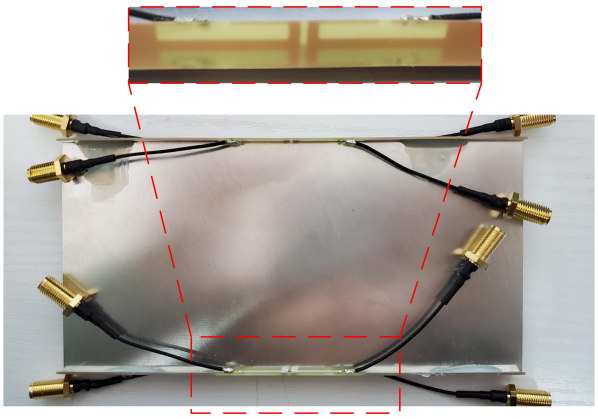

FIGURE 11. Photograph of the fabricated eight-element MIMO antenna prototype.

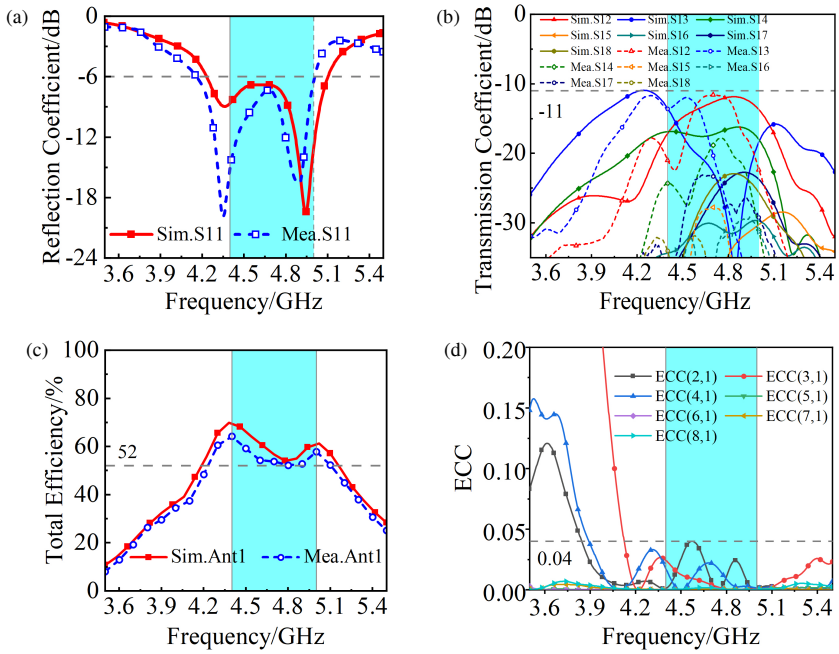

FIGURE 12. (a) Measured and simulated reflection coefficients. (b) Measured and simulated transmission coefficients. (c) Measured and simulated total efficiencies and (d) Measured ECC of the eight-element MIMO antenna.

and analyzed using Computer Simulation Technology (CST) software, with emphasis on evaluating its S-parameters, isolation, total efficiency, and radiation performance. Meanwhile, the corresponding measurements of the fabricated antenna were carried out using a vector network analyzer to validate the simulation results.

Due to the symmetry of the antenna layout, only a portion of the simulation and measurement results are presented in Figure 12. The measured and simulated results show good agreement. The MIMO antenna achieves a -6 dB impedance bandwidth ranging from 4.4 to 5.0 GHz, which fully covers the N79 frequency band. The minor deviations observed are primarily attributed to fabrication tolerances, soldering imperfections, and measurement uncertainties. The transmission coefficients between Ant 1 and the other seven antenna elements indicate that the isolation is greater than 11 dB throughout the entire frequency band. The antenna elements located in different modules, such as Ant 1 and Ant 5, exhibit weak electromagnetic coupling due to electromagnetic wave attenuation over the long transmission distance, thereby achieving high isolation. However, within the same module, the poor isolation between Ant 1 and Ant 2 at the higher resonant frequency, and between Ant 1 and Ant 3 at the lower resonant frequency, is mainly due to the strongly coupled currents at the feed points of adjacent antenna elements, induced by a single dominant mode. The measured efficiency results of the proposed antenna meet the requirements of 5G terminal communication, with Ant 1 maintaining a total efficiency above 52% and an average of 56%. The measured ECCs are below 0.04 over the operating band, which is significantly lower than the international standard of 0.5. Therefore, the proposed 8-element MIMO antenna exhibits good diversity performance. As shown in Figure 13, the normalized far-field radiation pattern of Ant 1 also confirms that the antenna exhibits favorable radiation characteristics.

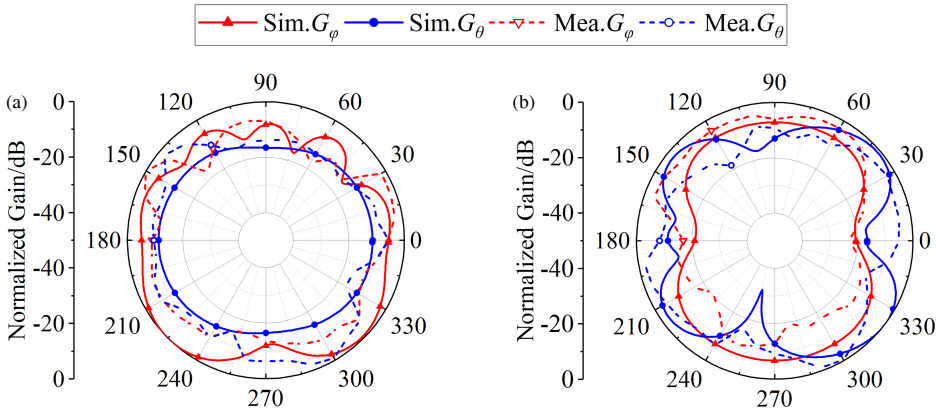

FIGURE 13. Simulated and measured normalized radiation patterns at 4.6 GHz: (a) XOY plane, (b) XOZ plane.

TABLE 1. Performance comparison of 5G MIMO antenna.

Ref.	Bandwidth (GHz)	Number of Elements	Antenna Size (mm^2)	Isolation (dB)	Total Efficiency (%)	Zero Ground Clearance
[17]	3.4–3.6	2	100×7	> 17	> 49	$\surd$
[19]	3.4–3.6	2	122.4×8	> 11	> 59	$\times$
[22]	3.4–3.6	4	28.6×25	> 15	> 51	$\times$
[26]	3.3–4.2	2	100×7.5	> 12	> 63	$\times$
This work	**4.4–5.0**	**4**	$\mathbf{43 \times 8}$	$\mathbf{> 11}$	$\mathbf{> 52}$	$\surd$

Table 1 provides a comparison between the proposed design and previously reported works, highlighting the superior characteristics of the four-antenna module for terminal applications. As shown in the table, the self-decoupled antenna pairs in [17, 19, 26] consist of only two antenna elements. To maintain high isolation between antenna pairs, these designs require relatively large spacing, resulting in an increased overall footprint of the MIMO antenna. In contrast, the design in [22] utilizes a four-element antenna group with elements placed symmetrically on both sides of the frame at reduced horizontal spacing. However, two antenna elements are positioned on the terminal back cover, thereby increasing the vertical height of the antenna structure and complicating its integration into terminal devices. In the proposed design, a compact four-antenna module, measuring merely $43 \times 8\,mm^2$, is integrated on each of the longer sides of the frame. Furthermore, the proposed antenna achieves an isolation better than 11 dB, a total efficiency exceeding 52%, and features a zero-clearance configuration. These results confirm the high performance of the antenna and its suitability for compact MIMO systems.

5. CONCLUSION

This paper presents a compact four-antenna module measuring merely $43 \times 8\,mm^2$, operating in the N79 band (4.4–5.0 GHz), and specifically designed for UAVs. By leveraging the partial cancellation of CM and DM currents, the antenna module achieves intrinsic self-decoupling without the need for additional decoupling structures, thereby minimizing design complexity and reducing overall size. Its zero-clearance layout is well suited for the constrained space of UAV platforms. By deploying a single module on each longer side of the frame, an eight-element MIMO antenna is realized. The proposed MIMO antenna achieves isolation greater than 11 dB between any two elements. The measured total efficiency exceeds 52% across the operating band, with an average of 56%. Combining a compact footprint, zero-clearance constraint, and high isolation, the proposed design offers a practical and efficient solution for integrating MIMO antenna in UAV-based 5G communication systems.

REFERENCES

[1] Andrews, J. G., S. Buzzi, W. Choi, S. V. Hanly, A. Lozano, A. C. K. Soong, and J. C. Zhang, "What will 5G be?" *IEEE Journal on Selected Areas in Communications*, Vol. 32, No. 6, 1065–1082, 2014.

[2] Dama, Y. A. S., R. A. Abd-Alhameed, S. M. R. Jones, D. Zhou, N. J. McEwan, M. B. Child, and P. S. Excell, "An envelope correlation formula for (N, N) MIMO antenna arrays using input scattering parameters, and including power losses," *International Journal of Antennas and Propagation*, Vol. 2011, No. 1, 421691, 2011.

[3] Hu, Y., W. Hong, C. Yu, Y. Yu, H. Zhang, Z. Yu, and N. Zhang, "A digital multibeam array with wide scanning angle and enhanced beam gain for millimeter-wave massive MIMO applications," *IEEE Transactions on Antennas and Propagation*, Vol. 66, No. 11, 5827–5837, 2018.

[4] Molisch, A. F. and M. Z. Win, "MIMO systems with antenna selection," *IEEE Microwave Magazine*, Vol. 5, No. 1, 46–56, 2004.

[5] Sun, L., Y. Li, Z. Zhang, and Z. Feng, "Wideband 5G MIMO antenna with integrated orthogonal-mode dual-antenna pairs for

metal-rimmed smartphones," *IEEE Transactions on Antennas and Propagation*, Vol. 68, No. 4, 2494–2503, 2020.

[6] Serghiou, D., M. Khalily, V. Singh, A. Araghi, and R. Tafazolli, "Sub-6 GHz dual-band 8 × 8 MIMO antenna for 5G smartphones," *IEEE Antennas and Wireless Propagation Letters*, Vol. 19, No. 9, 1546–1550, 2020.

[7] Megahed, A. A., M. Abdelazim, E. H. Abdelhay, and H. Y. M. Soliman, "Sub-6 GHz highly isolated wideband MIMO antenna arrays," *IEEE Access*, Vol. 10, 19 875–19 889, 2022.

[8] Gopal, K. V. and Y. S. Rao, "Mutual coupling reduction in UWB MIMO antenna using T-shaped stub," *Progress In Electromagnetics Research Letters*, Vol. 112, 77–85, 2023.

[9] Cui, L., J. Guo, Y. Liu, and C.-Y.-D. Sim, "An 8-element dual-band MIMO antenna with decoupling stub for 5G smartphone applications," *IEEE Antennas and Wireless Propagation Letters*, Vol. 18, No. 10, 2095–2099, 2019.

[10] Parchin, N. O., Y. I. A. Al-Yasir, A. H. Ali, I. Elfergani, J. M. Noras, J. Rodriguez, and R. A. Abd-Alhameed, "Eight-element dual-polarized MIMO slot antenna system for 5G smartphone applications," *IEEE Access*, Vol. 7, 15 612–15 622, 2019.

[11] Dong, J., S. Wang, and J. Mo, "Design of a twelve-port MIMO antenna system for multi-mode 4G/5G smartphone applications based on characteristic mode analysis," *IEEE Access*, Vol. 8, 90 751–90 759, 2020.

[12] Li, M., Y. Zhang, D. Wu, K. L. Yeung, L. Jiang, and R. Murch, "Decoupling and matching network for dual-band MIMO antennas," *IEEE Transactions on Antennas and Propagation*, Vol. 70, No. 3, 1764–1775, 2022.

[13] Cheor, W. L., A. A. Al-Hadi, P. J. Soh, M. F. Jamlos, A. M. Elshirkasi, X. Chen, and P. Akkaraekthalin, "A decoupling network for resonant and non-resonant sub-1 GHz MIMO mobile terminal antennas with improved compactness and efficiency," *IEEE Access*, Vol. 9, 59 475–59 485, 2021.

[14] Xu, Y., N. Li, C. Cui, X. Fan, J. Hou, and A. Wang, "A dual-band high-isolated MIMO antenna based on compensation network for 5G coal mine applications," *Progress In Electromagnetics Research Letters*, Vol. 123, 47–54, 2025.

[15] Wang, W., Y. Wu, W. Wang, and Y. Yang, "Isolation enhancement in dual-band monopole antenna for 5G applications," *IEEE Transactions on Circuits and Systems II: Express Briefs*, Vol. 68, No. 6, 1867–1871, 2021.

[16] Dong, J., X. Yu, and L. Deng, "A decoupled multiband dual-antenna system for WWAN/LTE smartphone applications," *IEEE Antennas and Wireless Propagation Letters*, Vol. 16, 1528–1532, 2017.

[17] Sun, L., H. Feng, Y. Li, and Z. Zhang, "Compact 5G MIMO mobile phone antennas with tightly arranged orthogonal-mode pairs," *IEEE Transactions on Antennas and Propagation*, Vol. 66, No. 11, 6364–6369, 2018.

[18] Hu, W., Z. Chen, L. Qian, L. Wen, Q. Luo, R. Xu, W. Jiang, and S. Gao, "Wideband back-cover antenna design using dual characteristic modes with high isolation for 5G MIMO smartphone," *IEEE Transactions on Antennas and Propagation*, Vol. 70, No. 7, 5254–5265, 2022.

[19] Ren, A., Y. Liu, and C.-Y.-D. Sim, "A compact building block with two shared-aperture antennas for eight-antenna mimo array in metal-rimmed smartphone," *IEEE Transactions on Antennas and Propagation*, Vol. 67, No. 10, 6430–6438, 2019.

[20] Zhao, X., S. P. Yeo, and L. C. Ong, "Decoupling of inverted-F antennas with high-order modes of ground plane for 5G mobile MIMO platform," *IEEE Transactions on Antennas and Propagation*, Vol. 66, No. 9, 4485–4495, 2018.

[21] Hu, W., Q. Li, H. Wu, Z. Chen, L. Wen, W. Jiang, and S. Gao, "Dual-band antenna pair with high isolation using multiple orthogonal modes for 5G smartphones," *IEEE Transactions on Antennas and Propagation*, Vol. 71, No. 2, 1949–1954, 2023.

[22] Pang, B., X. Ai, W. Hu, W. Jiang, and B. Lu, "Closely arranged self-decoupled MIMO antenna group using orthogonal mode and pattern diversity for 5G mobile terminals," *International Journal of RF and Microwave Computer-Aided Engineering*, Vol. 32, No. 11, e23372, 2022.

[23] Chang, L., Y. Yu, K. Wei, and H. Wang, "Polarization-orthogonal co-frequency dual antenna pair suitable for 5G MIMO smartphone with metallic bezels," *IEEE Transactions on Antennas and Propagation*, Vol. 67, No. 8, 5212–5220, 2019.

[24] Chang, L., Y. Yu, K. Wei, and H. Wang, "Orthogonally polarized dual antenna pair with high isolation and balanced high performance for 5G MIMO smartphone," *IEEE Transactions on Antennas and Propagation*, Vol. 68, No. 5, 3487–3495, 2020.

[25] Xu, H., S. Gao, H. Zhou, H. Wang, and Y. Cheng, "A highly-integrated MIMO antenna unit," in *2019 13th European Conference on Antennas and Propagation (EuCAP)*, 1–5, Krakow, Poland, 2019.

[26] Sun, L., Y. Li, Z. Zhang, and H. Wang, "Self-decoupled MIMO antenna pair with shared radiator for 5G smartphones," *IEEE Transactions on Antennas and Propagation*, Vol. 68, No. 5, 3423–3432, 2020.